Inorganic Hole Conducting Layers for Perovskite-Based Solar Cells

ARTICLE *in* JOURNAL OF PHYSICAL CHEMISTRY LETTERS · APRIL 2014

Impact Factor: 7.46 · DOI: 10.1021/jz500645n

6 AUTHORS, INCLUDING:

Anand Selvin Subbiah
Indian Institute of Technology Bombay
14 PUBLICATIONS **65** CITATIONS
SEE PROFILE

Ansuman Halder
Indian Institute of Technology Bombay
6 PUBLICATIONS **53** CITATIONS
SEE PROFILE

Soham Ghosh
Indian Institute of Technology Bombay
7 PUBLICATIONS **57** CITATIONS
SEE PROFILE

Neha Mahuli
Indian Institute of Technology Bombay
9 PUBLICATIONS **52** CITATIONS
SEE PROFILE

THE JOURNAL OF PHYSICAL CHEMISTRY Letters

Letter

pubs.acs.org/JPCL

Inorganic Hole Conducting Layers for Perovskite-Based Solar Cells

Anand S. Subbiah,[†] Ansuman Halder,[†] Soham Ghosh,[†] Neha Mahuli,[‡] Gary Hodes,[§] and Shaibal K. Sarkar*,[†]

[†]Department of Energy Science and Engineering, [‡]Center for Research in Nanotechnology and Science, Indian Institute of Technology Bombay, Powai, Mumbai, Maharashtra 400076, India

[§]Department of Materials and Interface, Weizmann Institute of Science, 76100 Rehovot, Israel

Supporting Information

ABSTRACT: Hybrid organic−inorganic semiconducting perovskite photovoltaic cells are usually coupled with organic hole conductors. Here, we report planar, inverse $CH_3NH_3PbI_{3-x}Cl_x$-based cells with inorganic hole conductors. Using electrodeposited NiO as hole conductor, we have achieved a power conversion efficiency of 7.3%. The maximum V_{OC} obtained was 935 mV with an average V_{OC} value being 785 mV. Preliminary results for similar cells using electrodeposited CuSCN as hole conductor resulted in devices up to 3.8% in efficiency. The ability to obtain promising cells using NiO and CuSCN expands the presently rather limited range of available hole conductors for perovskite cells.

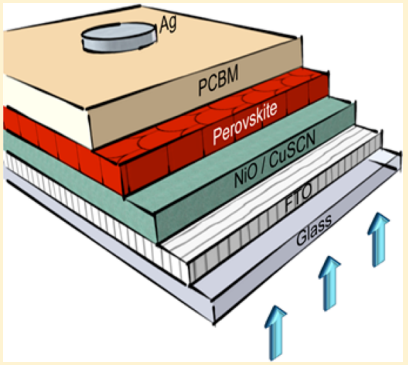

SECTION: Energy Conversion and Storage; Energy and Charge Transport

Solid-state hybrid organic−inorganic lead halide perovskite semiconductors have proven to be one of the most promising materials in low cost photovoltaics. A phenomenal increase in device performance has been achieved within a span of a few years.[1−6] Because of their excellent optoelectronic properties, including high mobility, long diffusion length, and long carrier lifetimes,[7−10] their successful implementation into both mesostructured and planar heterojunction architectures have resulted in energy conversion efficiencies close to 16%.[11,12]

In comparison with the other technologies that have taken decades to reach a point where they can be considered for commercialization, perovskite-based cells are approaching this state in an unprecedented manner.[1] The hybrid semiconductor thin film employed as the absorber material in various architectures can also be deposited by a range of deposition techniques such as spin-coating, two-step sequential deposition, vacuum evaporation, vapor assisted solution processes, and so forth.[11−16] Simple and low-energy fabrication procedures make them extremely favorable candidates for commercialization. Reports of the entire fabrication of high efficiency cells under 100 °C clearly depict the competitive edge for this technology.[12,17]

A typical PV device configuration employing methylammonium lead halide ($MAPbX_3$) as an absorber material most commonly uses TiO_2 as electron transport layer and an organic hole conducting layer. Several hole conducting organic materials have been employed, mostly depending on the specific perovskite (in particular, whether the iodide or bromide) and the device structure.[18,19]

Inorganic hole conductors have been much less used for perovskite cells. Christians et al.,[20] described the use of a CuI hole conductor with conversion efficiency of 6.0%. They also showed that unencapsulated CuI/perovskite cells showed better stability than corresponding spiro-OMeTAD ones. Inorganic NiO thin films have been employed successfully as a hole conducting material in p-type DSSC and OPV devices.[21−25] They have also been previously explored in inverse architecture perovskite-based solar cells with very low efficiency (ca. 0.05%)[26] and, very recently, using spin-coated NiO to give 7.8% cells.[27] Doctor-bladed CuSCN has also been recently used in a conventional-architecture perovskite cell (i.e., CuSCN deposited on the perovskite) with 4.85% efficiency reported.[28]

In this communication, we investigate electrodeposited NiO (and preliminary results using electrodeposited CuSCN) as hole-conductors in planar $CH_3NH_3PbI_{3-x}Cl_x$-based solar cells with inverse architecture (i.e., the perovskite is deposited on the hole conductor rather than the other way around). The p-i-n type device architecture consists of fluorine-doped tin oxide (FTO)-coated glass, electrodeposited hole conducting film of NiO (or CuSCN), vacuum evaporated perovskite absorber, and spin-coated [6,6]-phenyl-C61-butyric acid methyl ester (PCBM) with an evaporated silver contact (FTO/NiO/$CH_3NH_3PbI_{3-x}Cl_x$/PCBM/Ag). A maximum power conver-

Received: April 2, 2014
Accepted: April 30, 2014

   dx.doi.org/10.1021/jz500645n | J. Phys. Chem. Lett. 2014, 5, 1748−1753

sion efficiency (PCE) of 7.3% was obtained with NiO and 3.8% in preliminary experiments employing CuSCN.

The band energy diagram of the inverted architecture device employing NiO and CuSCN hole conductors is shown in Scheme 1. Though a wide range of HOMO positions have been reported for NiO in the literature, it is typically somewhat lower than that of CuSCN.

Scheme 1. Band Energy Diagram of NiO- and CuSCN-Based Perovskite Cells Used in This Study.[a]

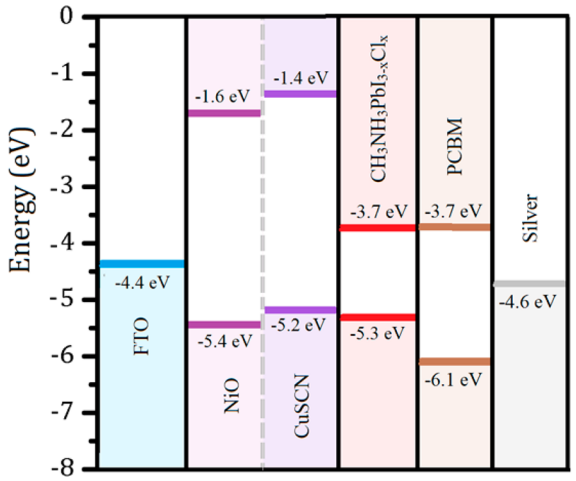

[a]The NiO valence band position is a roughly average value from the large variation found in the literature.

Photoluminescence (PL) quenching of the perovskite emission was carried out to study the compatibility of the hole conducting materials. For PL measurements, $CH_3NH_3PbI_{3-x}Cl_x$ films with thickness of ca. 250 nm were deposited on microscope glass slides, FTO-coated glass, FTO/NiO, and FTO/CuSCN substrates. The bandgap of the vapor deposited $CH_3NH_3PbI_{3-x}Cl_x$ film was determined from the direct bandgap Tauc plot and found to be 1.59 eV. For all PL measurements, an excitation wavelength of 530 nm was used. A broad PL emission peak at around 770 nm was found for the films on glass slides as shown in Figure 1. A considerable decrease in the PL intensities was observed when the perovskite was deposited either on FTO or on FTO/NiO. Apart from a small peak at 825 nm, no band-edge signal was observed for a film deposited on an FTO/CuSCN substrate. The PL quenching efficiency was found to be ca. 87% and 90% for FTO and NiO substrates, respectively, and >96% for CuSCN. Thus, the calculated PL quenching efficiency for inorganic hole conducting materials was comparable to that found for the traditionally used organic hole conductors reported earlier.[26]

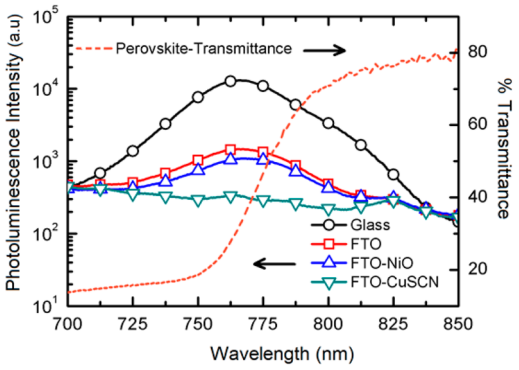

Figure 1. Photoluminescence of $CH_3NH_3PbI_{3-x}Cl_x$ coated on glass, FTO, FTO/NiO, and FTO/CuSCN showing their charge quenching characteristics together with the % transmittance spectrum of the perovskite (orange dashed curve).

For cell formation, the annealed NiO films were subjected to UV light treatment (UV light source UVC 254 nm, which forms O_3 in the presence of oxygen) before depositing the absorber layer. Cells fabricated without UV light treatment showed a low fill factor. O_2 plasma treatment of NiO has been shown to increase the NiO work function and give better organic photovoltaic devices, presumed due to surface oxidation.[29] UV/ozone treatments of various oxides were shown to have a similar effect to O_2 plasma treatment.[30]

Figure 2 shows a cross section SEM image of the inverse device architecture consisting of glass/FTO (bottom of image), NiO hole conducting layer with $CH_3NH_3PbI_{3-x}Cl_x$, and spin-coated PCBM as electron transport layer. The cross section SEM image also depicts a uniform deposition along the length of the device.

The $J-V$ curves of champion and average cells using NiO as hole conductor are shown in Figure 3a. The champion NiO-based perovskite cells exhibited a power conversion efficiency of 7.3%, a short circuit current (J_{SC}) of 14.2 mA/cm^2 and an open circuit voltage (V_{OC}) of 786 mV. Although this V_{OC} was similar to the average value, a maximum value of 935 mV was attained, comparable to V_{OC} values obtained using spiro-OMeTAD. The short circuit current, open circuit voltage, and other parameters were obtained from a batch size of 24 NiO-based perovskite solar cells, and the values are tabulated in Table 1. The champion NiO-based perovskite device performance is comparable to those reported earlier by Christians et al., using CuI as hole conductor[20] and the planar NiO devices published by Jeng et al. recently.[27]

We also made some cells without the NiO (i.e., the perovskite deposited directly on the FTO). Though reasonable, if somewhat lower values of J_{SC} and V_{OC} (8−10 mA cm^{-2} and 600−800 mV) were obtained, the fill factor was invariably <0.3. Some form of charge-selective contact seems to be necessary in this case.

From preliminary experiments using CuSCN instead of NiO, a conversion efficiency of 3.8% was obtained (Figure 4). The V_{OC} of 677 mV is on the low limit of those obtained from these cells, and a maximum value of 900 mV has been obtained in these preliminary experiments. Therefore, it seems likely that CuSCN will also turn out to be at least a reasonably good hole conductor for the iodide perovskites.

A simple one-diode model fit of the dark current voltage characteristics revealed that NiO-based cells exhibit a low series resistance value (R_S) compared to those using CuSCN. The best NiO cell showed an R_S of ca. 4.4 Ω cm^2, whereas the best CuSCN cell exhibited greater than an order of magnitude higher value of ca. 63 Ω cm^2. In addition, the typical shunt resistance (R_{SH}) is about an order of magnitude higher for the average NiO-based cells ($R_{SH} \sim 800$ Ω cm^2) than for CuSCN-based ones (~70 Ω cm^2). Thus, despite CuSCN showing a higher quenching ability than NiO, they exhibit a poorer photovoltaic performance. However, it is too early to know if this is an intrinsic difference or due to less experience with the perovskite−CuSCN combination.

To investigate the electrical properties of the electro-deposited inorganic hole transport materials, current−voltage

dx.doi.org/10.1021/jz500645n | J. Phys. Chem. Lett. 2014, 5, 1748−1753

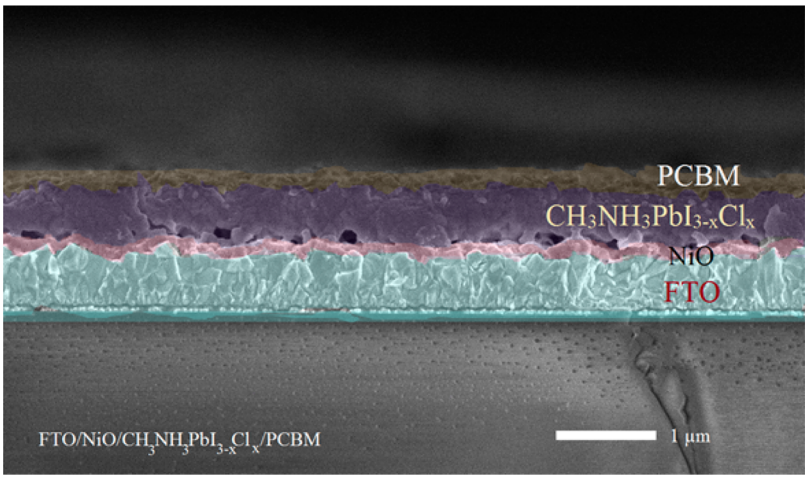

Figure 2. SEM cross section of the optimized NiO-based inverse architecture perovskite cells where the distinct layers are highlighted in different colors. The Ag contact is not shown here.

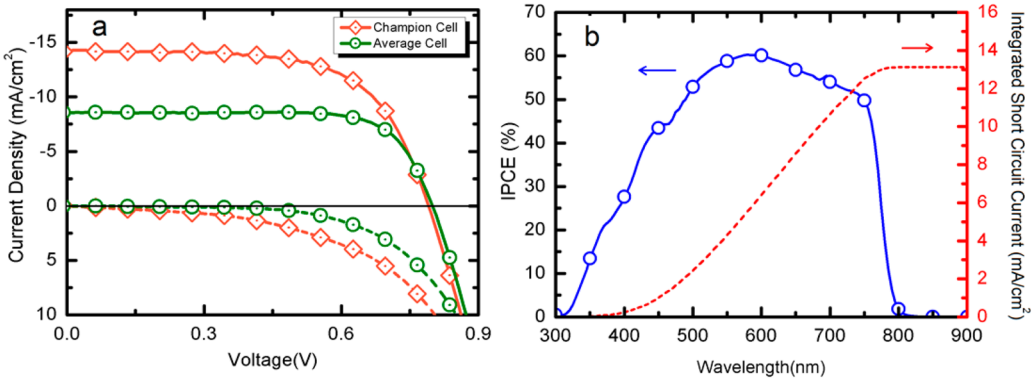

Figure 3. (a) Current voltage characteristics of the champion FTO/NiO/$CH_3NH_3PbI_{3-x}Cl_x$/PCBM/Ag cell (diamonds) and an average characteristic (circles) from a batch of 24 cells (see Table 1 and Figure SI 1 in Supporting Information for statistical data of those cells) using Xe lamp irradiation calibrated to 100 mW/cm^2. The corresponding dark characteristics are given by dashed lines. (b) IPCE of a comparable NiO-based device and the corresponding integrated short circuit current over the spectrum.

Table 1. Champion Cell, Mean, and Maximum Photovoltaic Parameters of a Batch of FTO/NiO/$CH_3NH_3PbI_{3-x}Cl_x$/PCBM/Ag Cells[a]

hole transport material		J_{SC} (mA/cm^2)	V_{OC} (mV)	fill factor (FF)	PCE % (η)
nickel oxide (NiO)	champion	14.2	786	0.65	7.26
	mean ± SD	9.6 ± 3.2	784 ± 50	0.62 ± 0.07	4.7 ± 1.7
	maximum	14.9	936	0.75	7.26

[a]The mean values and standard deviations are calculated from a batch of 24 cells and a summary of their distribution is given in Figure SI 1 (Supporting Information).

characteristics were obtained by sandwiching NiO or CuSCN films between FTO and Au contacts. Dark $I-V$ characteristics showed a good diode behavior for NiO films of thickness 100 nm as shown in Figure 5 with low series and relatively high shunt resistances (Table 2). CuSCN showed a much poorer diode behavior that depended strongly on the CuSCN thickness. In fact, the CuSCN shows no clear blocking behavior except for the thickest (600 nm) film, suggesting that the shunting of the thinner films might be due to direct shorting paths through the thinner CuSCN. However, the high series resistance of the CuSCN films will degrade the device performance.

However, the impact of high series resistance of the CuSCN layer in the complete planar device architecture under dark conditions is considerably reduced upon illumination (see Figure 4). The CuSCN-based cell series resistance dropped to 7.4 Ω cm^2 under illumination from 63 Ω cm^2 in the dark, showing that upon hole injection from the absorber layer, the resistance of the material is decreased. It should be noted that CuSCN-based cells also exhibit a crossover of dark and light JV characteristics, unlike NiO-based devices (compare Figures 3 and 4). Although there are a number of possible reasons for this, the hole injection mechanism (indirect photoconduction) is the simplest explanation.

In conclusion, we have shown that NiO and, to a lesser extent (at present), CuSCN inorganic hole conductors can serve as potentially feasible replacements for the organic hole conductors in perovskite solar cells. The use of inverse cell structures allows relatively high temperature processing, and the use of deposition techniques that would be incompatible

dx.doi.org/10.1021/jz500645n | J. Phys. Chem. Lett. 2014, 5, 1748−1753

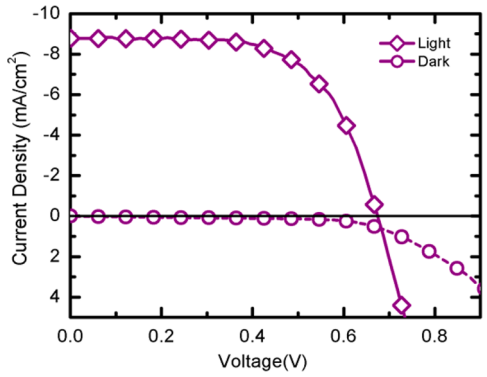

Figure 4. Light and dark $J-V$ characteristics of a FTO/CuSCN/$CH_3NH_3PbI_{3-x}Cl_x$/PCBM/Ag cell.

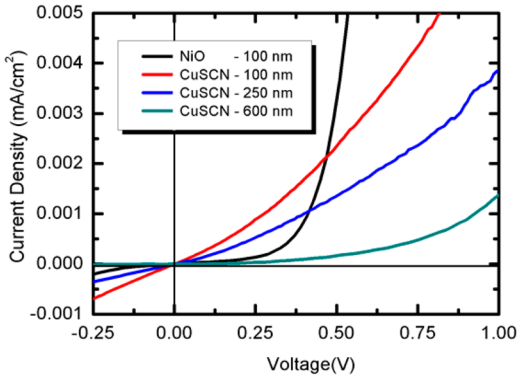

Figure 5. Dark $I-V$ characteristics of FTO/NiO(100 nm)/Au and FTO/CuSCN/Au (100, 250, and 600 nm thick CuSCN).

Table 2. Series and Shunt Resistance Values Extracted from the $I-V$ Characteristics of Figure 5

device structure	R_S (Ω cm^2)	R_{SH} (Ω cm^2)
FTO/NiO(100 nm)/Au	1.46	2510
FTO/CuSCN(100 nm)/Au	92.2	480
FTO/CuSCN(250 nm)/Au	218	500
FTO/CuSCN(600 nm)/Au	230	62 000

with the perovskite materials in a normal (hole conductor deposited on the perovskite) structure. Though the absolute conversion efficiencies reported here are well below those of state-of-the-art perovskite cells, they represent a promising step toward further development. It is important to mention that all the device syntheses were performed under ambient conditions where the average humidity was higher than that normally encountered. Although we have not carried out stability studies so far, the use of inorganic layers for both electron and hole transport layers might protect the moisture-sensitive perovskite absorber better than organic materials (the latter often are also oxygen sensitive).

EXPERIMENTAL SECTION

MATERIALS REQUIRED

Fluorine-doped tin oxide coated glass (Pilkington, TEC-8), nickel nitrate hexahydrate (Merck, 98%), copper sulfate pentahydrate (Merck, 98%), Titriplex III (ethylenedinitrilotetraacetic acid disodium salt dihydrate) (Merck, >99%), potassium thiocyanate (Fisher Scientific, 97%), methylamine (Merck, 40% solution in water), hydriodic acid (57 wt % in water), lead chloride (Aldrich, 98%), [6,6]-phenyl-C61-butyric acid methyl ester (PCBM) (Aldrich, 99%), (1,3)-dimethyl-2-phenyl-(2,3)-dihydro-1H-benzimidazole (DMBI) (Aldrich, 97%), silver metal (Parekh Industries, 99.99%), and chlorobenzene (Sigma-Aldrich, 99.9%) were used as supplied without further processing.

Substrate Preparation. FTO substrates were cut to a 3 × 1 cm size and cleaned with Alconox solution followed by rinsing with double-distilled water. Then the substrates were subjected to ultrasonication in Alconox solution, followed by isopropanol, acetone, and Millipore water for a period of 30 min each. The cleaned substrates were then dried in a dry air stream.

Electrodeposition of NiO Films. Nickel oxide films were deposited on top of the FTO substrates (working electrode) by galvanostatic electrodeposition in a three electrode system with a platinum rod counter electrode and Ag/AgCl reference electrode. A thin layer of $Ni(OH)_2$ was initially deposited in a 0.02 M aqueous $NiNO_3$ bath with a constant current density of ~0.25 mA/cm^2 for 2 min. The $Ni(OH)_2$ thin films were then dried and annealed at 350 °C for 1 h in air in a muffle furnace to form NiO films of approximately 100 nm thickness. The films appeared nonporous but with high surface roughness. Annealing at a temperature higher than 400 °C resulted in a highly resistive NiO layer, whereas only partial conversion could be achieved if annealed at temperatures below 250 °C. Before deposition of the absorber layer on top of the NiO electrode, the sample was subjected to UV light treatment for approximately 20 min.

Electrodeposition of CuSCN Films. Orthorhombic CuSCN films were deposited by potentiostatic electrodeposition[31] at −0.4 V with respect to the Ag/AgCl reference electrode, with a platinum rod counter electrode and FTO-coated glass as working electrode. The composition of the deposition bath was 0.04 M $CuSO_4$, 0.04 M Titriplex ($C_{10}H_{14}N_2Na_2O_8.2H_2O$), and 0.02 M KSCN in aqueous solution, and the pH of this solution was at 1.8. No postdeposition annealing was employed. The deposition conditions were chosen to deposit nonporous films rather than a 3D architecture.

Synthesis of Methylammonium Iodide. Methylammonium iodide was synthesized by reacting 27.86 mL of methylamine (40% solution in water) in 100 mL of ethanol with 30 mL of hydriodic acid (57 wt % in water) in a round-bottom flask. The reaction was stirred in an ice bath for a period of 2 h.[15] Then, the solvent was evaporated using a rotary evaporator and the product recrystallized from a mixture of ethanol and diethyl ether (1:1 by volume). The crystallized methylammonium iodide was washed repeatedly twice with diethyl ether and dried in vacuum at 60 °C for 20 h. The sample was then stored in a dark atmosphere and used over a period of no more than 2 weeks.

Coevaporation of $CH_3NH_3PbI_{3-x}Cl_x$. The mixed halide perovskite absorber was deposited via dual source vacuum evaporation by evaporating $PbCl_2$ and CH_3NH_3I precursors simultaneously. For the thin film monitor, the density of $PbCl_2$ was set to be 5.85 g/cm^3 and that of CH_3NH_3I 1.0 g/cm^3 as reported earlier,[11] and the tooling factors calculated accordingly. The $PbCl_2$ was evaporated at a rate of 0.95 ± 0.15 A/s and the CH_3NH_3I at 8.5 ± 1.5 A/s, resulting in a $PbCl_2$:CH_3NH_3I molar ratio of 1:5.4. The substrate temperature was held at a higher temperature than ambient (ca. 50

dx.doi.org/10.1021/jz500645n | J. Phys. Chem. Lett. 2014, 5, 1748−1753

°C) during the entire deposition process. The base pressure in the evaporation chamber was 7×10^{-6} mbar. The evaporation time was optimized for the best performing devices to be 24 and 18 min for NiO and CuSCN substrates, respectively, resulting in an absorber thickness varying between 250 and 500 nm. The films were then annealed in ambient at 90 °C for 60 min and the samples were subsequently subjected to deposition of PCBM followed by evaporation of silver contacts.

Spin Coating of PCBM. The PCBM precursor was prepared by dissolving 13 mg of [6,6]-phenyl-C61-butyric acid methyl ester (PCBM) in 1 mL of chlorobenzene. After stirring the solution for 5 min, 0.26 mg of (1,3)-dimethyl-2-phenyl-(2,3)-dihydro-1H-benzimidazole (DMBI) was added to the solution, and then the solution stirred continuously for 4 h. This precursor solution was then spin-coated at 3200 rpm on top of the FTO−(NiO/CuSCN)−$CH_3NH_3PbI_{3-x}Cl_x$ substrates for 30 s, and the samples were annealed at 80 °C in air for 5 min.

Silver Evaporation. The device fabrication was completed by thermally evaporating a 100 nm silver contact on top of the PCBM layer. A shadow mask with a 3 mm diameter was employed for this fabrication process, resulting in an active cell area of 0.07 cm^2. Al was also tried as contact material but was found to diffuse into the cell within a short time.

Measurements and Characterization. The UV−vis−NIR absorption measurements were performed using a PerkinElmer LAMBDA 950 spectrophotometer. Photoluminescence measurements were carried out on a JASCO FP-8200 fluorescence spectrometer. The external quantum efficiency or incident photon to converted electron (IPCE) ratio was measured using a Bentham PVE300 photovoltaic characterization system with a silicon photodiode detector in DC mode. The current voltage characteristics was measured by a Keithley 2400 using LAB Tracer software and the illumination was provided by means of a Newport variable power xenon lamp, calibrated to 100 mW/cm^2 light intensity, and the active area of 0.07 cm^2 was illuminated by employing a metal mask. The cross section images were obtained from JEOL JSM-7600F scanning electron microscope with a field emission electron gun.

■ ASSOCIATED CONTENT

Ⓢ Supporting Information

The distribution of the photovoltaic parameters obtained for the NiO devices. This material is available free of charge via the Internet at http://pubs.acs.org

■ AUTHOR INFORMATION

Corresponding Author

*E-mail: shaibal.sarkar@iitb.ac.in.

Notes

The authors declare no competing financial interest.

■ ACKNOWLEDGMENTS

The authors thank the National Center for Photovoltaic Research and Education aided by the Ministry of New and Renewable Energy, Government of India, for financial support.

■ REFERENCES

(1) Kamat, P. V. Evolution of Perovskite Photovoltaics and Decrease in Energy Payback Time. *J. Phys. Chem. Lett.* **2013**, *4*, 3733−3734.
(2) Hodes, G.; Cahen, D. Photovoltaics: Perovskite Cells Roll Forward. *Nat. Photonics* **2014**, *8*, 87−88.
(3) Hodes, G. Perovskite-based Solar Cells. *Science* **2013**, *342*, 317−318.
(4) Bisquert, J. The Swift Surge of Perovskite Photovoltaics. *J. Phys. Chem. Lett.* **2013**, *4*, 2597−2598.
(5) Park, N.-G. Organometal Perovskite Light Absorbers Toward a 20% Efficiency Low-Cost Solid-State Mesoscopic Solar Cell. *J. Phys. Chem. Lett.* **2013**, *4*, 2423−2429.
(6) Snaith, H. J. Perovskites: The Emergence of a New Era for Low-Cost, High-Efficiency Solar Cells. *J. Phys. Chem. Lett.* **2013**, *4*, 3623−3630.
(7) Stranks, S. D.; Eperon, G. E.; Grancini, G.; Menelaou, C.; Alcocer, M. J. P.; Leijtens, T.; Herz, L. M.; Petrozza, A.; Snaith, H. J. Electron-Hole Diffusion Lengths Exceeding 1 Micrometer in an Organometal Trihalide Perovskite Absorber. *Science* **2013**, *342*, 341−344.
(8) Kim, H.-S.; Mora-Sero, I.; Gonzalez-Pedro, V.; Fabregat-Santiago, F.; Juarez-Perez, E. J.; Park, N.-G.; Bisquert, J. Mechanism of Carrier Accumulation in Perovskite Thin-Absorber Solar Cells. *Nat. Commun.* **2013**, *4*, 2242.
(9) Xing, G.; Mathews, N.; Sun, S.; Lim, S. S.; Lam, Y. M.; Grätzel, M.; Mhaisalkar, S.; Sum, T. C. Long-Range Balanced Electron- and Hole-Transport Lengths in Organic-Inorganic $CH_3NH_3PbI_3$. *Science* **2013**, *342*, 344−347.
(10) Zhao, Y.; Nardes, A. M.; Zhu, K. Solid-State Mesostructured Perovskite $CH_3NH_3PbI_3$ Solar Cells: Charge Transport, Recombination, and Diffusion Length. *J. Phys. Chem. Lett.* **2014**, *5*, 490−494.
(11) Liu, M.; Johnston, M. B.; Snaith, H. J. Efficient Planar Heterojunction Perovskite Solar Cells by Vapour Deposition. *Nature* **2013**, *501*, 395−398.
(12) Liu, D.; Kelly, T. L. Perovskite Solar Cells with a Planar Heterojunction Structure Prepared Using Room-Temperature Solution Processing Techniques. *Nat. Photonics* **2014**, *8*, 133−138.
(13) Burschka, J.; Pellet, N.; Moon, S.-J.; Humphry-Baker, R.; Gao, P.; Nazeeruddin, M. K.; Gratzel, M. Sequential Deposition as a Route to High-Performance Perovskite-Sensitized Solar Cells. *Nature* **2013**, *499*, 316−319.
(14) Lee, M. M.; Teuscher, J.; Miyasaka, T.; Murakami, T. N.; Snaith, H. J. Efficient Hybrid Solar Cells Based on Meso-Superstructured Organometal Halide Perovskites. *Science* **2012**, *338*, 643−647.
(15) Noh, J. H.; Im, S. H.; Heo, J. H.; Mandal, T. N.; Seok, S. I. Chemical Management for Colorful, Efficient, and Stable Inorganic−Organic Hybrid Nanostructured Solar Cells. *Nano Lett.* **2013**, *13*, 1764−1769.
(16) Chen, Q.; Zhou, H.; Hong, Z.; Luo, S.; Duan, H.-S.; Wang, H.-H.; Liu, Y.; Li, G.; Yang, Y. Planar Heterojunction Perovskite Solar Cells via Vapor-Assisted Solution Process. *J. Am. Chem. Soc.* **2013**, *136*, 622−625.
(17) Malinkiewicz, O.; Yella, A.; Lee, Y. H.; Espallargas, G. M.; Graetzel, M.; Nazeeruddin, M. K.; Bolink, H. J. Perovskite Solar Cells Employing Organic Charge-Transport Layers. *Nat. Photonics* **2014**, *8*, 128−132.
(18) Edri, E.; Kirmayer, S.; Henning, A.; Mukhopadhyay, S.; Gartsman, K.; Rosenwaks, Y.; Hodes, G.; Cahen, D. Why Lead Methylammonium Tri-Iodide Perovskite-Based Solar Cells Require a Mesoporous Electron Transporting Scaffold (but Not Necessarily a Hole Conductor). *Nano Lett.* **2014**, *14*, 1000−1004.
(19) Heo, J. H.; Im, S. H.; Noh, J. H.; Mandal, T. N.; Lim, C.-S.; Chang, J. A.; Lee, Y. H.; Kim, H.-J.; Sarkar, A.; Nazeeruddin Md, K.; et al. Efficient Inorganic-Organic Hybrid Heterojunction Solar Cells Containing Perovskite Compound and Polymeric Hole Conductors. *Nat. Photonics* **2013**, *7*, 486−491.
(20) Christians, J. A.; Fung, R. C. M.; Kamat, P. V. An Inorganic Hole Conductor for Organo-Lead Halide Perovskite Solar Cells. Improved Hole Conductivity with Copper Iodide. *J. Am. Chem. Soc.* **2013**, *136*, 758−764.
(21) Li, L.; Gibson, E. A.; Qin, P.; Boschloo, G.; Gorlov, M.; Hagfeldt, A.; Sun, L. Double-Layered NiO Photocathodes for p-Type DSSCs with Record IPCE. *Adv. Mater.* **2010**, *22*, 1759−1762.

(22) Odobel, F.; Le Pleux, L. C.; Pellegrin, Y.; Blart, E. New Photovoltaic Devices Based on the Sensitization of p-Type Semiconductors: Challenges and Opportunities. *Acc. Chem. Res.* **2010**, *43*, 1063−1071.
(23) Manders, J. R.; Tsang, S.-W.; Hartel, M. J.; Lai, T.-H.; Chen, S.; Amb, C. M.; Reynolds, J. R.; So, F. Solution-Processed Nickel Oxide Hole Transport Layers in High Efficiency Polymer Photovoltaic Cells. *Adv. Funct. Mater.* **2013**, *23*, 2993−3001.
(24) Irwin, M. D.; Buchholz, D. B.; Hains, A. W.; Chang, R. P. H.; Marks, T. J. p-Type Semiconducting Nickel Oxide as an Efficiency-Enhancing Anode Interfacial Layer in Polymer Bulk-Heterojunction Solar Cells. *Proc. Nat. Acad. Sci.* **2008**, *105*, 2783−2787.
(25) Shim, J. W.; Fuentes-Hernandez, C.; Dindar, A.; Zhou, Y.; Khan, T. M.; Kippelen, B. Polymer Solar Cells with NiO Hole-Collecting Interlayers Processed by Atomic Layer Deposition. *Org. Elec.* **2013**, *14*, 2802−2808.
(26) Docampo, P.; Ball, J. M.; Darwich, M.; Eperon, G. E.; Snaith, H. J. Efficient Organometal Trihalide Perovskite Planar-Heterojunction Solar Cells on Flexible Polymer Substrates. *Nat. Commun.* **2013**, *4*, 2761.
(27) Jeng, J.-Y.; Chen, K.-C.; Chiang, T.-Y.; Lin, P.-Y.; Tsai, T.-D.; Chang, Y.-C.; Guo, T.-F.; Chen, P.; Wen, T.-C.; Hsu, Y.-J. Nickel Oxide Electrode Interlayer in $CH_3NH_3PbI_3$ Perovskite/PCBM Planar-Heterojunction Hybrid Solar Cells. *Adv. Mater.* **2014**, in press.
(28) Ito, S.; Tanaka, S.; Vahlman, H.; Nishino, H.; Manabe, K.; Lund, P. Carbon-Double-Bond-Free Printed Solar Cells from TiO_2/$CH_3NH_3PbI_3$/CuSCN/Au: Structural Control and Photoaging Effects. *ChemPhysChem* **2014**, *15*, 1194−1200.
(29) Steirer, K. X.; Chesin, J. P.; Widjonarko, N. E.; Berry, J. J.; Miedaner, A.; Ginley, D. S.; Olson, D. C. Solution Deposited NiO Thin-Films as Hole Transport Layers in Organic Photovoltaics. *Org. Elec.* **2010**, *11*, 1414−1418.
(30) Wang, Z. B.; Helander, M. G.; Greiner, M. T.; Qiu, J.; Lu, Z. H. Analysis of Charge-Injection Characteristics at Electrode-Organic Interfaces: Case Study of Transition-Metal Oxides. *Phys. Rev. B: Condens. Matter Mater. Phys.* **2009**, *80*, 235325.
(31) Ni, Y.; Jin, Z.; Fu, Y. Electrodeposition of p-Type CuSCN Thin Films by a New Aqueous Electrolyte With Triethanolamine Chelation. *J. Am. Ceram. Soc.* **2007**, *90*, 2966−2973.